Arabian Journal of Chemistry (2020) 13, 4035–4042

King Saud University

Arabian Journal of Chemistry

www.ksu.edu.sa
www.sciencedirect.com

ORIGINAL ARTICLE

A solvent-dependent fabrication of flower-like and hexagonally ring-like ZnO architectures in one minute

Yan Bao [a,b,*], Lu Gao [a,c], Caiping Feng [a,c], Jianzhong Ma [a,*], Chao Liu [d], Wenbo Zhang [d]

[a] College of Bioresources Chemical and Materials Engineering, Shaanxi University of Science and Technology, Xi'an 710021, China
[b] Shaanxi Research Institute of Agricultural Products Processing Technology, Xi'an 710021, China
[c] National Demonstration Center for Experimental Light Chemistry Engineering Education, Shaanxi University of Science and Technology, Xi'an 710021, China
[d] Shaanxi Collaborative Innovation Center of Industrial Auxiliary Chemistry and Technology, Shaanxi University of Science and Technology, Xi'an 710021, China

Received 10 April 2019; accepted 7 June 2019
Available online 14 June 2019

KEYWORDS

Flower-like ZnO;
Hexagonally ring-like ZnO;
One minute;
Solvent process

Abstract Flower-like ZnO and hexagonally ring-like ZnO nanomaterials were fabricated via a triethylamine assisted solvent process free from any other auxiliary chemicals. Like magic, this process could be implemented just in one minute without any laboratory apparatus. More importantly, the flower-like ZnO was transformed into hexagonally ring-like ZnO as the content of additional water was changed from 10% to 0%. The fast nucleation and morphological evolution of ZnO superstructures could be mainly attributed to surface-self-assembly and base-erosion process. The designed fabrication procedure is simple, feasible, and universal for ZnO with controlled microstructure and improved performances.

1. Introduction

Zinc oxide (ZnO) is one of the fascinating nanomaterials that can be used in numerous technological fields, due to its enthralling physicochemical properties that includes a wide band gap (3.37 eV), considerable excitation binding energy at room temperature (60 meV), high optical transparency in the visible region, strong piezoelectricity, environmentally friendly and so on (Wang et al., 2017; Dilger et al., 2014; Zhao et al., 2013; Mao et al., 2018; Wang et al., 2015; Maiti et al., 2013). As we all known, the morphologies of ZnO nanomaterials

* Corresponding authors at: College of Bioresources Chemical and Materials Engineering, Shaanxi University of Science and Technology, Xi'an 710021, China (Y. Bao).
E-mail addresses: baoyan@sust.edu.cn (Y. Bao), majz@sust.edu.cn (J. Ma).

Peer review under responsibility of King Saud University.

Production and hosting by Elsevier

https://doi.org/10.1016/j.arabjc.2019.06.003
1878-5352

have a profound influence on their properties. Therefore, design and tailor of ZnO nanomaterials with different morphologies and superstructures are very important in view of both basic fundamental research and development of novel devices (Liu et al., 2016; Maiti et al., 2015; Lu et al., 2016). To meet the demand for practical applications, various ZnO nanostructures have been fabricated, including 0D hollow spheres, 1D nanorods and nanowires, 2D nanosheets and 3D hierarchical architectures (Liu et al., 2014; Park et al., 2012; Lin et al., 2016; Wang et al., 2012; Dai et al., 2013).

To date, various methodologies have been developed to fabricate various special superstructures, such as thermal evaporation, chemical vapor deposition (CVD), microwave technologies, hydrothermal, solvothermal, sonochemical methods and so on (Yue et al., 2012; Meng, et al., 2015; Hu, et al., 2011; Wang et al., 2014; Wang et al., 2013; Zang et al., 2015). However, those methods usually need diversified high experiment apparatus, a complex and time-consuming synthesis process and so on. So it is still significant to develop novel, low-cost and rapid routes to synthesize extraordinary ZnO nanomaterials.

In this work, flower-like ZnO and hexagonally ring-like ZnO nanomaterials were creatively fabricated via a triethylamine assisted solvent process free from any other auxiliary chemicals. Like magic, this process could be implemented at room temperature just in one minute without any laboratory apparatus, avoiding the defects of existing methods, such as time-consuming, complex processing. Significantly, the morphology of flower-like ZnO and hexagonally ring-like ZnO possess excellent reproducibility. Hence, this fabrication method opens a brand new field for synthesizing the similar particular superstructures of ZnO nanomaterials or other complex systems. More importantly, the fast nucleation and morphological evolution of ZnO superstructures could be mainly attributed to surface-self-assembly and base-erosion process.

2. Experiment section

2.1. Synthesis of ZnO architectures

All reagents were analytical grade. A novel, one minute process was employed to fabricate flower-like and hexagonally ring-like ZnO architectures. In a typical run for flower-like ZnO, 5 mmol Zn $(CH_3COO)_2{\cdot}2H_2O$ was directly dissolved into the deionized water with vigorously stirring until a homogeneous clear solution. Then, the triethylamine (TEA) was dropped into the above solution at room temperature (RT). The content of additional water was about 10%, while the total volume of TEA-H_2O mixture solution was kept constant at 50 mL. After being stirred for one minute, a large amount of white colored precipitate was separated out immediately. Ultimately, the resultant white colored precipitate was collected and washed several times with deionized water to remove the possible residues, and then dried under the oven at 60 °C for 6 h. The same procedure as for the preparation of flower-like ZnO was used for the synthesis of hexagonally ring-like ZnO, except that the content of additional water was decreased to 0%.

2.2. Characterization

The crystalline phase of the ZnO products was identified by powder X-ray diffraction (XRD) analysis using a D/max 2550 V diffractometer with Cu Kα radiation (λ = 1.5406 Å, Rigaku, Tokyo, Japan), and the XRD data were collected at a scanning rate of 0.021°/s for 2θ in a range from 20° to 80°. The microstructures of the as-obtained ZnO products were observed using a Hitachi S-4800 field emission scanning electron microscopy (FESEM). Transmission electron microscopy (TEM) and high-resolution TEM (TEM/HRTEM, Tecnai G^2, FEI) were also used to assess the morphologies and crystalline structure of the ZnO products. The Brunauer-Emmett-Teller (BET) surface area of the ZnO products were analyzed by nitrogen adsorption-desorption isotherms determined at liquid nitrogen temperature on an automatic analyzer (ASAP 2460).

3. Results and discussion

Fig. 1 shows the typical FESEM images of the flower-like ZnO and hexagonally ring-like ZnO superstructures prepared in one minute assisted by triethylamine. As can be seen from Fig. 1a, the flower-like ZnO structures were synthesized successfully with 10% water content in mixture solvents. The size of the flower-like structures is on the scale of micrometers with a diameter of about 1–1.5 μm. The high-magnification FESEM image (inset of Fig. 1a) reveals that each flower-like ZnO is consisted of closely packed rugby-shaped structures with lengths of 350–600 nm. Interestingly, the flower-like ZnO

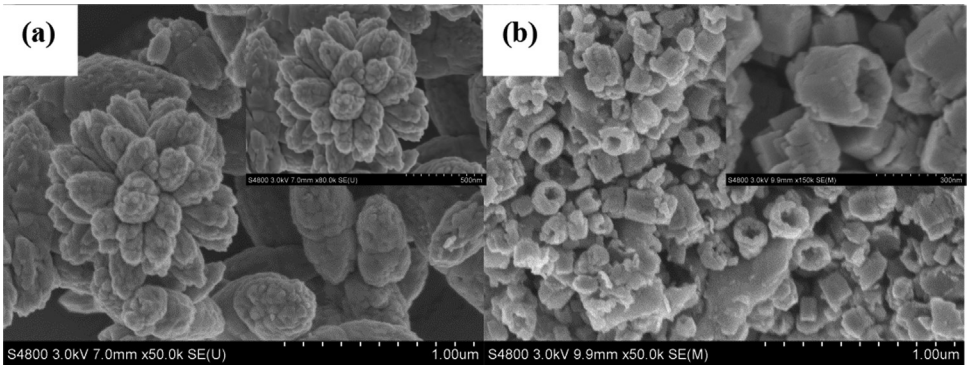

Fig. 1 FESEM images of (a) flower-like ZnO and (b) hexagonally ring-like ZnO, the inset is an enlarged SEM image of the corresponding ZnO products.

was transformed into hexagonally ring-like ZnO as the content of additional water was changed from 10% to 0%, as shown in Fig. 1b. A clear hollow architecture of hexagonally ring-like ZnO is also observed. The average outer-diameter and length of the hexagonally ring-like ZnO are about 250 and 300 nm, respectively. However, a more distinct variation was observed with further modified of water content to 50%, showing that the well-dispersed rugby-shaped ZnO was fabricated (Fig. S1). These observations suggest that the water content in mixture solvents could strongly affect the nucleation as well as the growth processes of ZnO crystals in one minute, resulting in different morphologies evolution of ZnO nanomaterials.

To evaluate the morphological reproducibility of flower-like ZnO and hexagonally ring-like ZnO, three times of preparative experiments were performed repeatedly. Fig. S2 shows the FESEM images of the flower-like ZnO and hexagonally ring-like ZnO fabricated via three times of repeated experiments. It is noteworthy that repeated experiments have been carried out by keeping any reaction parameters constant entirely. It can be clearly seen that the morphology of flower-like ZnO and hexagonally ring-like ZnO possess excellent reproducibility.

To verify the phase composition and structural properties of the samples prepared with 10% and 0% water content in mixture solvents, x-ray diffraction analyses were carried out. Fig. 2 shows the XRD patterns of the as-synthesized ZnO structures with different morphologies. As can be seen, all of the observed diffraction peaks of the ZnO samples matched well with those from standard hexagonal wurtzite structured ZnO (JCPDS no. 36-1451). Its relatively sharp and strong peaks suggest that the ZnO phase is of highly crystalline. No other crystalline phase corresponding to impurity was detected, which indicates that the flower-like and hexagonally ring-like structures are all pure-phase ZnO. As shown in Fig. 2, the ZnO microstructures have similar XRD patterns, with differences in their relative peak intensities due to their random orientation. The strong (1 0 0) and (1 0 1) diffraction peaks suggest that ⟨1 0 0⟩ and ⟨1 0 1⟩ are the preferred growth orientations of the flower-like ZnO (Fig. 2a). As for hexagonally ring-like ZnO (Fig. 2b), the preferred growth orientations is about ⟨1 0 0⟩, ⟨0 0 2⟩ and ⟨1 0 1⟩.

The microstructures and surface area of the flower-like ZnO and hexagonally ring-like ZnO were characterized by Brunauer–Emmett–Teller (BET) nitrogen desorption/adsorption isotherms, including specific surface area, pore volume and pore size. As shown in Fig. 3a and b, the flower-like ZnO and hexagonally ring-like ZnO exhibit a hysteresis loop at relative pressure range of 0.7–0.9, which can be classified as type III adsorption isotherms according to the International Union of Pure and Applied Chemistry (IUPAC) classification. This type of hysteresis loop reveals the existence of abundant mesoporous structures in ZnO microstructures. The obtained specific data are presented in Table 1. As can be seen, the specific surface area of the flower-like ZnO and hexagonally ring-like ZnO are 14.15 and 17.12 $m^2 g^{-1}$, respectively. The larger specific surface area possessed by the hexagonally ring-like ZnO samples is mainly due to the smaller size and prominent hollow degree of ZnO structures.

The detailed morphologies and microstructures of the ZnO products were investigated by TEM and HRTEM. The TEM image (Fig. 4a) further confirms that the flower-like ZnO architectures are constructed by radial rugby-shaped rod arrays from the center to the surface of the flower. The HRTEM image in Fig. 4c indicates a rugby-like ZnO nanorod in the "flower-like" structure, with clear lattice fringes at a d-spacing of 0.26 nm, corresponding to the (0 0 2) lattice plane of hexagonal ZnO. Namely, the preferred growth orientation of the flower-like ZnO is parallel to (0 0 0 1). The corresponding selected area electron diffraction (SAED) pattern, shown in the Fig. 4e, indicates that the flower-like ZnO structures are monocrystal in nature and are indexed as the hexagonal ZnO phase in accordance with the XRD data. Fig. 4b shows TEM image of hexagonally-like ZnO with a "ring-like" structure, while the lattice fringes at a d-spacing of 0.28 nm, corresponding to the (1 0 0) spacing of wurtzite-ZnO are depicted in Fig. 4d. The Fig. 4f confirms that the hexagonally ring-like structures are single crystals and are grown along the c-axis direction.

The specific experimental operation has a crucial influence on morphology of flower-like ZnO and hexagonally ring-like ZnO. Fig. S3 shows the FESEM images of the ZnO samples prepared with the following three operations: (a) triethylamine

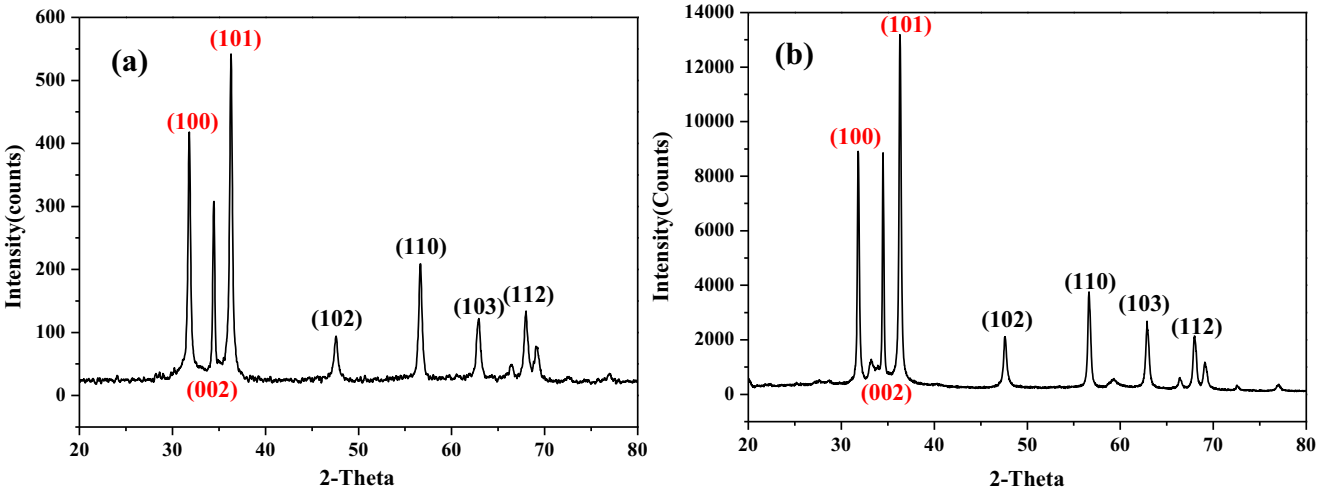

Fig. 2 XRD patterns of (a) flower-like ZnO and (b) hexagonally ring-like ZnO.

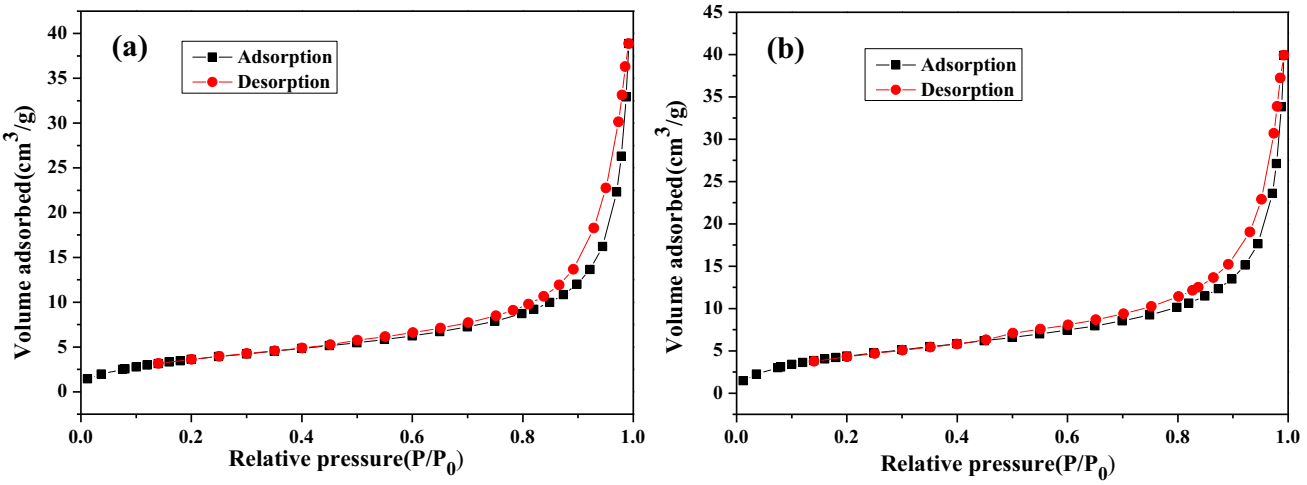

Fig. 3 The nitrogen adsorption-desorption isotherms of (a) flower-like ZnO and (b) hexagonally ring-like ZnO.

Table 1 Specific surface area, pore volume, average pore size of various ZnO microstructures.

Sample	S_{BET}[a] ($m^2\ g^{-1}$)	Pore volume[b] ($cm^3\ g^{-1}$)	Pore size[c] (nm)
Flower-like ZnO	14.15	0.06	17.13
Hexagonally ring-like ZnO	17.12	0.06	15.18

[a] The BET surface area is calculated from the linear part of the BET plot (P/P_0 = 0.05–0.3).
[b] Pore volume is determined by adsorption branch of the nitrogen isotherms at P/P_0 = 0.994.
[c] Average pore size is estimated using the adsorption branch of the nitrogen isotherms and the Barrett-Joyner-Halenda method.

joined directly, (b) triethylamine added dropwise, (c) solution of zinc acetate dihydrate added dropwise. And it is noteworthy that the water content in mixture solvents is all about 10%. As can be seen from Fig. S3a, the flower-like ZnO were fabricated successfully via triethylamine joined directly. When addition manner of triethylamine changed from joining directly to adding dropwise, the petal of flower-like ZnO was entirely scattered, and the conus-like ZnO was fabricated extensively (Fig. S3b). By farther changing the addition manner of the solution of zinc acetate dihydrate to adding dropwise, a clear granular architecture was fabricated (Fig. S3c). These results show that adding dropwise can observably delay reaction degree of TEA with zinc ions, influencing the formation of flower-like ZnO in one minute. But the sudden addition of enough TEA can promote a large amount of zinc ions convert into ZnO. Fig. S4 shows the FESEM images of the ZnO samples grown in 0% water content with three different operations, (a) triethylamine joined directly, (b) triethylamine added dropwise, (c) zinc acetate dihydrate powder added dropwise, respectively. As can be seen from Fig. S4a, the hexagonally ring-like ZnO were fabricated successfully via triethylamine joined directly. As addition manner of triethylamine changed from joining directly to adding dropwise, the double-conus-like ZnO was fabricated extensively (Fig. S4b). This is consistent with the experimental results of flower-like ZnO. Accompanying with changing the addition manner of zinc acetate dehydrate powder to adding dropwise, laminar microstructure with well tightness can be produced on a large scale (Fig. S4c). XRD pattern (Fig. S5) of the above-mentioned laminar product indicates that it is not only hexagonal wurtzite structured ZnO, but also includes $Zn(OH)_2$ partly.

Based on the above analysis, the formation mechanism of flower-like ZnO and hexagonally ring-like ZnO is assigned to the surface-self-assembly at 10% water content and base-erosion at 0% water content, respectively (Fig. 5). In the whole fabrication process, TEA plays an important role in controlling the ZnO superstructures (Long et al., 2010). Firstly, it is speculated that the presence of TEA blocks the preferential growth of ZnO crystals along the C-axis. Namely, the TEA molecules acted as a structure-directing agent are adsorbed on the surface of the ZnO crystal core and then impel neighboring starting nuclei randomly aggregated together to form a spherical aggregation. In addition, TEA assists in the hydrolysis of zinc acetate dihydrate to form ZnO, even without additional water in the reaction system. Obviously, the formation of manifold ZnO superstructures depends on the added amounts of TEA and deionized water into the reaction solution profoundly. When the water content is maintained at 10%, a high concentration of TEA and a proper amount of deionized water lead to a fast nucleation and congregation of ZnO crystal, resulting in the rugby-like ZnO nanorods plentifully. To minimize surface energy of the system, rugby-like ZnO nanorods assemble to form flower-like ZnO, which explain the basis of the growth mechanism of flower-like ZnO when water content is about 10%. The van der waals force interactions between the surface molecules of the rugby-like ZnO nanorods could be perceived as the driving force for self-assembly. However, when the water content is increased from 10% to 50%, rugby-shaped ZnO just can be formed by the isotropic growth from center nuclei on account of the low concentration of TEA in mixture solvents. Contrarily, as the water content is reduced from 10% to 0%, a low growth rate would result in quasi-equilibrium growth of ZnO nanocrystal owing to only TEA in solvent. The diethylzinc adduct combines with TEA and Zn^{2+} is widely used as a precursor for the growth of ZnS, ZnSe and ZnO, for the reason

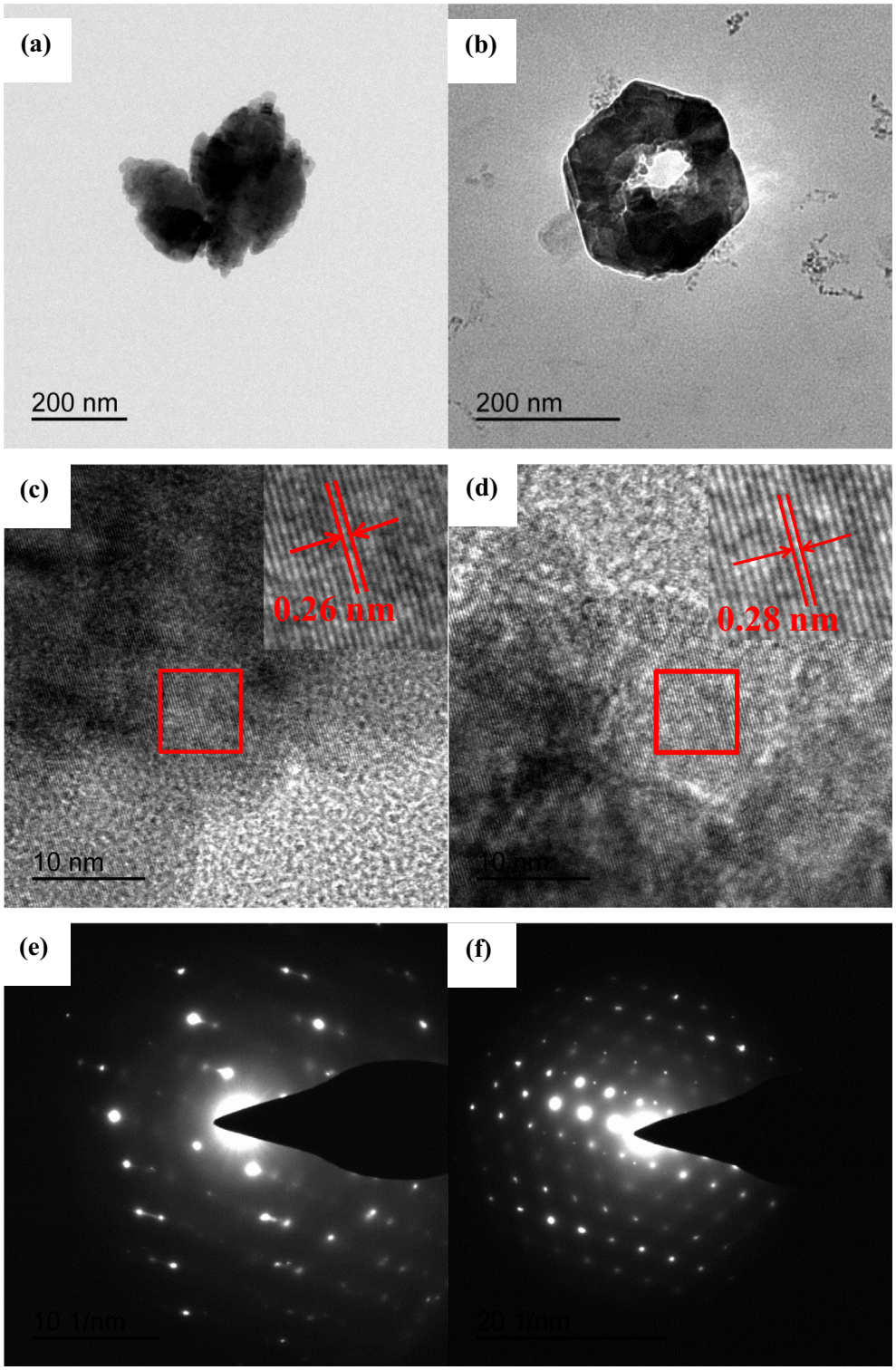

Fig. 4 TEM images of (a) flower-like ZnO and (b) hexagonal ring-like ZnO, their corresponding (c and d) HRTEM images and (e and f) SAED patterns.

that TEA as the stabilizer has a capacity for coordinating with Zn^{2+} ions, as reported (Jones et al., 1991). Thus, the initial nucleation just in the TEA solution could provide a kinetically favorable condition and stabilize structure of Zn-(0 0 0 1) plane, which generates the regular hexagonal ZnO prisms. As we all known, the distinct overdosage alkaline TEA possess a sufficient pH level, which makes the hexagonally-like ZnO erode from the center point to the outside in succession (Zeng et al., 2017). At the center of the hexagonally-like ZnO, the local zinc concentration is the highest, causing the

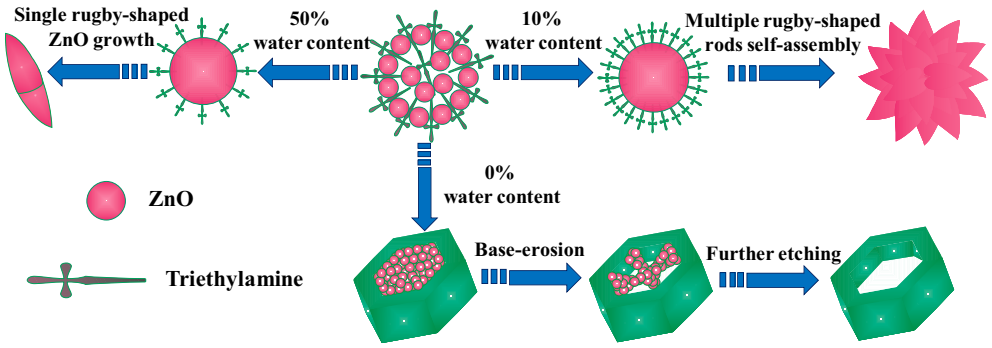

Fig. 5 Schematic illustration of the flower-like ZnO and hexagonal ring-like ZnO.

Table 2 A summary of flower-like ZnO and ring-like ZnO reported in literatures.

Morphologies	Methods	Alkali source	Structure directing agents	Reaction conditions	Ref
Flower-like ZnO	Wet-chemical	NaOH	Sodium ascorbate	60 °C, 3 h	Raula, et al., 2010
Flower-like ZnO	Hydrothermal	NaOH	Sodium citrate	180 °C, 6 h	Zhang, et al., 2015
Flower-like ZnO	Hydrothermal	NaOH	Ethanolamine	140 °C, 12 h	Wang, et al., 2011
Flower-like ZnO	Hydrothermal	NaOH	Citric acid	150 °C, 19 h	Mao, et al., 2019
Flower-like ZnO	Solvothermal	NaOH	Polyethyleneglycol	110 °C, 10 h	Agarwal, et al., 2019
Flower-like ZnO	Supercritical assisted solvothermal	–	–	120 °C, 24 h	Wang et al., 2013
Flower-like ZnO	Sonication	Ammonia	TEA	80 °C, 3 h	Cheng, et al., 2008
Hexagonally ring-like ZnO	Hydrothermal	NaOH	Ionic liquid ([C_3mim]Br)	120 °C, 24 h	Lian, et al., 2011
Hexagonally ring-like ZnO	Hydrothermal	–	–	150 °C, 12 h	Qi, et al., 2013
Ring-like ZnO	Thermal evaporation	–	–	900 °C, 2 h	Wu, et al., 2009
Flower-like ZnO and hexagonally ring-like ZnO	Wet-chemical	TEA	TEA	RT, 1 min	Our work

fastest erosion velocity of the center of the hexagonally-like ZnO. Therefore, when the water content is decreased to 0%, the hexagonally ring-like ZnO tends to be formed at the erosion effect of extra base.

To further confirm the superiority of the method used in our work, a summary about reaction conditions and the materials used in preparation of flower-like ZnO and ring-like ZnO reported in the literatures are shown in Table 2. It can be seen that various methods have been developed to obtain flower-like ZnO and ring-like ZnO. However, compared with the method used in our work, these methods require a long time at a high temperature, extra alkali source and the addition of structure directing agents. Moreover, the realization of morphology transformation between flower-like ZnO and ring-like ZnO using the same method has not been reported in the literatures.

4. Conclusion

Herein, we ingeniously synthesized flower-like ZnO and hexagonally ring-like ZnO nanomaterials via a triethylamine assisted solvent process free from any other auxiliary chemicals. Like magic, this process could be implemented just in one minute without any laboratory apparatus. More importantly, the flower-like ZnO was transformed into hexagonally ring-like ZnO as the content of additional water was changed form 10% to 0%. A mechanism that comprises surface-self-assembly at 10% water content and base-erosion at 0% water content to form flower-like ZnO and hexagonally ring-like ZnO is proposed, respectively. The solvolysis based one minute fabrication approach can also be applied to new and other material and material combinations or be used for more specific shape control purposes. We are sure that many interesting questions about this particle synthesis process are still ahead of us and the interested scientific community.

Acknowledgements

Thanks for the supports from the National Natural Science Foundation of China (No: 21878181), the Key Research and Development Program of Shaanxi Province (No: 2018ZDXM-GY-118) and the Key Scientific Research Group of Shaanxi Province (No: 2013KCT-08).

Appendix A. Supplementary material

Supplementary data to this article can be found online at https://doi.org/10.1016/j.arabjc.2019.06.003.

References

Agarwal, S., Rai, P., Gatellc, E.N., Llobet, E., Güelle, F., Kumar, M., Awasthi, K., 2019. Gas sensing properties of ZnO nanostructures (flowers/rods) synthesized by hydrothermal method. Sens. Actuators, B. 292, 24–31. https://doi.org/10.1016/j.snb.2019.04.083.

Cheng, B., Wang, X.F., Liu, L.Y., Guo, L.T., 2008. Growth mechanism and morphology dependent luminescence properties of ZnO nanostructures prepared in aqueous solution. Mater. Lett. 62, 3099–3102. https://doi.org/10.1016/j.matlet.2008.01.115.

Dai, J., Xu, C.X., Xu, X.Y., Guo, J.Y., Li, J.T., Zhu, G.Y., Lin, Y., 2013. Single ZnO microrod ultraviolet photodetector with high photocurrent gain. ACS Appl. Mater. Interfaces 5, 9344–9348. https://doi.org/10.1021/am403609y.

Dilger, S., Wessig, M., Wagner, M.R., Reparaz, J.S., Sotomayor Torres, C.M., Qijun, L., Dekorsy, T., Polarz, S., 2014. Nanoarchitecture effects on persistent room temperature photoconductivity and thermal conductivity in ceramic semiconductors: mesoporous, yolk-shell, and hollow ZnO spheres. Cryst. Growth Des. 14, 4593–4601. https://doi.org/10.1021/cg500680g.

Hu, J., Chen, M., Fang, X.S., Wu, L.M., 2011. Fabrication and application of inorganic hollow spheres. Chem. Soc. Rev. 40, 5472–5491. https://doi.org/10.1039/C1CS15103G.

Jones, A.C., Wright, P.J., Cockayne, B., 1991. Precursors for II–VI semiconductors: requirements and developments. J. Cryst. Growth 107, 297–308. https://doi.org/10.1016/0022-0248(91)90474-j. (Jones et al., 1991)22.

Lian, J.B., Ding, Z.M., Kwong, F.L., Ng, Dickon H.L., 2011. Template-free hydrothermal synthesis of hexagonal ZnO microcups and micro-rings assembled by nanoparticles. Crystengcomm 13, 4820–4822. https://doi.org/10.1039/c1ce05301a.

Lin, X., Chen, M., 2016. Fabrication and photo-detecting performance of 2D ZnO inverse opal films. Appl. Sci. 6, 259. https://doi.org/10.3390/app6100259.

Liu, H.J., Zang, Z.G., Tang, X.S., 2014. Synthesis mechanism and optical properties of well nanoflower-shaped ZnO fabricated by a facile method. Opt. Mater. Express. 4, 1762–1769. https://doi.org/10.1364/OME.4.001762.

Liu, X.D., Ye, L.Q., Liu, S.S., Li, Y.P., Ji, X.X., 2016. Photocatalytic reduction of CO2 by ZnO micro/nanomaterials with different morphologies and ratios of 0001 Facets. Sci. Rep. 6, 38474. https://doi.org/10.1038/srep38474.

Long, T.F., Dong, X.L., Liu, X.W., Liu, J.X., Yin, S., Sato, T., 2010. Synthesis of ZnO crystals with unique morphologies by a low-temperature solvothermal process and their photocatalytic deNOx properties. Res. Chem. Intermed. 36, 61–67. https://doi.org/10.1007/s11164-010-0114-9.

Lu, M.Y., Chen, H.Y., Tsai, C.Y., Tseng, Y.T., Kuo, Y.T., Wang, H. C., Lu, M.P., 2016. Low-temperature-grown p-n ZnO nanojunction arrays as rapid and self-driven UV photodetectors. Chem. Commun. 52, 12853–12856. https://doi.org/10.1039/C6CC06347K.

Maiti, S., Maiti, U.N., Behera, B.C., Pala, S., Chattopadhyay, K.K., 2013. Controlling the sharpness of ZnO tetrapods by restricted zinc oxidation in the open air: a low turn-on field emitter stabilized by graphene. J. Mater. Chem. C. 1, 4940–4947. https://doi.org/10.1039/C3TC30775A.

Maiti, S., Pal, S., Chattopadhyay, K.K., 2015. Recent advances in low temperature, solution processed morphology tailored ZnO nanoarchitectures for electron emission and photocatalysis applications. CrystEngComm. 17, 9264–9295. https://doi.org/10.1039/C5CE01130B.

Mao, Y.Q., Li, Y.H., Zou, Y.J., Shen, X.Y., Zhu, L.P., Liao, G.H., 2019. Solvothermal synthesis and photocatalytic properties of ZnO micro/nanostructures. Ceram. Int. 45, 1724–1729. https://doi.org/10.1016/j.ceramint.2018.10.054.

Mao, Y.T., Wang, Q., Wu, X., Xie, H.Q., Ma, X.M., Chen, M., 2018. Continuous carbon hollow shell with ZnO nanoparticles embedded as anode material with superior lithium storage capability. Energy Technol. 6, 188–195. https://doi.org/10.1002/ente.201700397.

Meng, F.L., Hou, N.N., Jin, Z., Sun, B., Guo, Z., Kong, L.T., Xiao, X.H., Wu, H., Li, M.Q., Liu, J.H., 2015. Ag-decorated ultra-thin porous single-crystalline ZnO nanosheets prepared by sunlight induced solvent reduction and their highly sensitive detection of ethanol. Sens. Actuators, B. 209, 975–982. https://doi.org/10.1016/j.snb.2014.12.078.

Park, S., An, S., Ko, H., Jin, C., Lee, C., 2012. Synthesis of nanograined ZnO nanowires and their enhanced gas sensing properties. ACS Appl. Mater. Interf. 4, 3650–3656. https://doi.org/10.1021/am300741r.

Qi, K.Z., Yang, J.Q., Fu, J.Q., Wang, G.C., Zhu, L.J., Liu, G., Zheng, W.J., 2013. Morphology-controllable ZnO rings: ionic liquid-assisted hydrothermal synthesis, growth mechanism and photoluminescence properties. CrystEngComm 15, 6729–6735. https://doi.org/10.1039/c3ce27007f.

Raula, M., Rashid, M.H., Paira, T.K., Dinda, E., Mandal, T.K., 2010. Ascorbate-assisted growth of hierarchical ZnO nanostructures: Sphere, spindle, and flower and their catalytic properties. Langmuir 26, 8769–8782. https://doi.org/10.1021/la904507q.

Wang, L., Yu, L.J., Yi, L.T., Yuan, B., Hou, Y.P., Meng, X.F., Liu, J., 2017. Long time and distance self-propelling of a PVC sphere on a water surface with an embedded ZnO micro-/nano-structured hollow sphere. Chem. Commun. 53, 2347–2350. https://doi.org/10.1039/C6CC09308F.

Wang, L., Ma, C., Ru, X.L., Guo, Z., Wu, D.P., Yu, G.H., Hu, Y.S., Wang, J.S., 2015. Facile synthesis of ZnO hollow microspheres and their high performance in photocatalytic degradation and dye sensitized solar cells. J. Alloys Compd. 647, 57–62. https://doi.org/10.1016/j.jallcom.2015.05.086.

Wang, M.H., Sun, Z.K., Yue, Q., Yang, J., Sun, Z.K., Yue, Q., Yang, J., Wang, X.Q., Deng, Y.H., Yu, C.Z., Zhao, D.Y., 2014. An interface-directed co-assembly approach to synthesize uniform large-pore mesoporous silica spheres. J. Am. Chem. Soc. 136, 1884–1892. https://doi.org/10.1021/ja4099356.

Wang, M., Zhao, B., Xu, S.H., Lin, L., Liu, S.J., He, D.N., 2013. Synthesis of hierarchically structured ZnO nanomaterials via a supercritical assisted solvothermal process. Chem. Commun. 50, 930–932. https://doi.org/10.1039/c3cc48306a.

Wang, X.J., Zhang, Q.L., Wan, Q., Dai, G.Z., Zou, B.S., 2011. Controllable ZnO architectures by ethanolamine-assisted hydrothermal reaction for enhanced photocatalytic activity. J. Phys. Chem. C. 115, 2769–2775. https://doi.org/10.1021/jp1096822.

Wang, X.Z., Liu, W., Liu, J.R., Wang, F.L., Kong, J., Qiu, S., He, C. Z., Luan, L.Q., 2012. Synthesis of nestlike ZnO hierarchically porous structures and analysis of their gas sensing properties. ACS Appl. Mater. Interf. 4, 817–825. https://doi.org/10.1021/am201476b.

Wu, X., Qu, F.Y., Zhang, X., Cai, W., Shen, G.Z., 2009. Fabrication of ZnO ring-like nanostructures at a moderate temperature via a thermal evaporation process. J. Alloys Compd. 486, L13–L16. https://doi.org/10.1016/j.jallcom.2009.06.197.

Yue, Q., Wang, M.H., Wei, J., Deng, Y.H., Liu, T.Y., Che, R.C., Tu, B., Zhao, D.Y., 2012. A template carbonization strategy to synthesize ordered mesoporous silica microspheres with trapped sulfonated carbon nanoparticles for efficient catalysis. Angew. Chem. 51, 10368–10372. https://doi.org/10.1002/anie.201204719.

Zang, Z.G., Wen, M.Q., Chen, W.W., Zeng, Y.F., Zu, Z.Q., Zeng, X. F., Tang, X.S., 2015. Strong yellow emission of ZnO hollow nanospheres fabricated using polystyrene spheres as templates. Mater. Des. 84, 418–421. https://doi.org/10.1016/j.matdes.2015.06.141.

Zeng, B.R., Zhang, L.C., Wu, L.Q., Lv, Y., 2017. Enclosed hollow tubular ZnO: Controllable synthesis and their high performance cataluminescence gas sensing of H_2S. Sens. Actuators, B. 242, 1086–1094. https://doi.org/10.1016/j.snb.2016.09.141.

Zhao, J., Li, J., Ying, P.L., Zhang, W.H., Meng, L.J., Li, C., 2013. Facile synthesis of freestanding Si nanowire arrays by one-step template-free electro-deoxidation of SiO_2 in a molten salt. Chem. Commun. 49, 4477–4479. https://doi.org/10.1039/C3CC00101F.

Zhang, Y., Liu, T.M., Hao, J.H., Lin, L.Y., Zeng, W., Peng, X.H., Wang, Z.H., 2015. Enhancement of NH_3 sensing performance in flower-like ZnO nanostructures and their growth mechanism. Appl. Surf. Sci. 357, 31–36. https://doi.org/10.1016/j.apsusc.2015.08.170.